

## Screening and band bending effects in the Stark control of electrons at interfaces (SCELI)

Antonio J. Garzón-Ramírez <sup>1</sup>, Francisco Fernández Villoria <sup>1,2</sup> and Ignacio Franco <sup>1,3,\*</sup>

<sup>1</sup>*Department of Chemistry, University of Rochester, Rochester, New York 14627, USA*

<sup>2</sup>*Departamento de Química, Módulo 13, Universidad Autónoma de Madrid, 28049 Madrid, Spain*

<sup>3</sup>*Department of Physics, University of Rochester, Rochester, New York 14627, USA*



(Received 20 October 2020; revised 11 May 2021; accepted 24 May 2021; published 4 June 2021)

Recently, we developed a general laser control scheme, i.e., the Stark control of electrons at interfaces (SCELI), based on Stark shifts, that is able to manipulate the electron dynamics at material interfaces [A. J. Garzón-Ramírez and I. Franco, *Phys. Rev. B* **98**, 121305 (2018)]. Here, we investigate how SCELI is influenced by the band bending effects introduced by interfacial dipoles and by the laser screening due to the polarization response of the material. For this, we follow the quantum dynamics of a model one-dimensional tight-binding semiconductor-semiconductor heterojunction driven by nonresonant few-cycle laser pulses of intermediate intensity. Band bending effects are introduced through an interfacial electrostatic potential term dictated by the depletion approximation of a neutral  $p$ - $n$  junction. In turn, screening effects are captured through the general boundary conditions of the field vectors at interfaces dictated by Maxwell's equations. For field amplitudes where SCELI dominates ( $E_0 \leq 0.55$  V/Å in the model), laser screening leads to a 46% reduction of the effect that can be partially compensated by increasing the intensity of the incident field. Surprisingly, band bending mildly affects SCELI. When both band bending and screening are considered simultaneously, the charge transfer is reduced, on average, 40% for  $E_0 \leq 0.46$  V/Å. Overall, we observe that screening and band bending change the magnitude of SCELI but leave the underlying mechanism for electron transfer intact.

DOI: [10.1103/PhysRevB.103.235304](https://doi.org/10.1103/PhysRevB.103.235304)

### I. INTRODUCTION

Controlling electron dynamics using lasers is an essential goal of science and technology [1–6]. This is because lasers allow manipulation of electrons on an ultrafast timescale [7–31], opening new ways to control the ability of matter to chemically react [32–39], conduct charge [8–12,18,23,26,28,30,31,40–48], absorb light [49–53], or other properties on a femto- to attosecond timescale.

Recently, we introduced a general scheme for the Stark control of electrons at interfaces (SCELI) [28]. The scenario is based on using nonresonant few-cycle laser pulses of intermediate intensity (nonperturbative but nonionizing) to distort the electronic structure and create transient resonances among the valence band (VB) levels and the conduction band (CB) levels of two adjacent materials through Stark effects. These transient resonances open laser-controllable quantum tunneling pathways for interfacial electron transfer. The reason to use a few-cycle laser is because it allows for the use of strong fields with intensity  $\sim 10^{13}$  W/cm<sup>2</sup> that lead to nontrivial Stark effects before the onset of dielectric breakdown [12,29,54].

The Stark effect refers to the shifts of energy levels in matter due to the application of an electric field. Stark routes for the control of electrons are a form of Hamiltonian control [13,28,37–39,48,55–57] based on pushing energy levels around. That is, on modifying the Hamiltonian by using the response of matter to strong nonresonant light. The advan-

tage of Stark routes for control of electrons is that they can be used even in the presence of strong decoherence [28,48] because they do not exploit the fragile coherence properties of electronic superposition states. This feature of Stark-based schemes of control is crucial as the electronic decoherence in matter is remarkably fast (typically  $\sim 10$  fs) [58–61].

Thus far, the investigation of SCELI [28,48] has been based on idealized models where the band lineup of the heterojunction is not affected by interfacial dipoles and where the electric field due to the photogenerated dipole is not taken into account. However, in realistic systems, once an interface is formed, thermal equilibrium leads to an interfacial dipole as a result of the charge migration at the interface. This interfacial dipole, in turn, creates a potential barrier against electron or hole transfer [62–67]. Further, the response of matter to light leads to an oscillating dipole [31,68–71] with an associated electric field that screens the incident electric field of light [31,70,71]. Currently, it is unclear to what extent SCELI will be affected, or even if it will survive, in the presence of these effects.

To address this problem, here we study SCELI including the screening and band bending effects on a model  $AB$  heterojunction composed of two adjacent one-dimensional two-band tight-binding semiconductors, and focus on the exemplifying case in which the two materials have no spectral overlap. To capture the screening, we use a self-consistent model in which the incident light is screened by the instantaneous electric polarization of the system. This polarization is the result of the charge displacement due to the interaction of the electronic cloud of the heterojunction with the laser field. In turn, the

\*ignacio.franco@rochester.edu

effects of band bending are introduced through an electrostatic profile at the interface given by the depletion approximation [72,73] for a neutral  $p$ - $n$  junction at thermal equilibrium.

This paper is organized as follows: Sec. II describes the tight-binding Hamiltonian for the  $AB$  heterojunction and the method employed to solve the time-dependent Schrödinger equation during and after photoexcitation. Section III details how SCELl is affected by band bending and screening effects. Our main results are summarized in Sec. IV.

## II. MODEL AND METHODS

As in Ref. [28], we study the electron transfer across the semiconductor-semiconductor interface. This interface is modeled as a one-dimensional insulating  $AB$  heterojunction with Hamiltonian

$$\hat{H} = \hat{H}_A + \hat{H}_B + \hat{H}_{AB}. \quad (1)$$

Here,  $\hat{H}_i$  is the Hamiltonian for material  $i = A$  or  $B$ , and  $\hat{H}_{AB}$  is their interfacial coupling. Each material is modeled as a two-band system with  $N_i = 50$  unit cells in dipole interaction with a laser field  $\mathbf{E}(t) = E(t)\hat{i}$ ,

$$\hat{H}_i = \sum_{n=1}^{2N_i} [h_{nn}^i + |e|E(t)x_n] \hat{a}_n^\dagger \hat{a}_n + \sum_{\langle n,m \rangle} h_{nm}^i (\hat{a}_n^\dagger \hat{a}_m + \text{H.c.}), \quad (2)$$

where  $\langle n, m \rangle$  denotes nearest neighbors, H.c. is the Hermitian conjugate, and the direction of laser polarization  $\hat{i}$  is chosen to be normal to the interfacial plane. Here,  $\hat{a}_n$  ( $\hat{a}_n^\dagger$ ) annihilates (creates) a fermion in site or Wannier function  $n$ ,  $\hat{a}_n^\dagger |0\rangle = |n\rangle$  where  $|0\rangle$  is the vacuum state, and satisfies the usual fermionic anticommutation relations. Each unit cell has two Wannier functions with alternating on-site energies ( $h_{nn}^i = h_{\text{even}}^i \delta_{n,\text{even}} + h_{\text{odd}}^i \delta_{n,\text{odd}}$ ) in tight-binding coupling among them ( $h_{n,n+1}^i = t_{\text{even}}^i \delta_{n,\text{even}} + t_{\text{odd}}^i \delta_{n,\text{odd}}$ ). Here,  $x_n$  denotes the position of each Wannier function along the junction and  $|e|$  the electron charge. The interaction between the semiconductors at the interface is given by  $\hat{H}_{AB} = -t_{AB}(\hat{a}_{2N_A}^\dagger \hat{a}_{2N_A+1} + \text{H.c.})$ , where  $t_{AB}$  is the interfacial tight-binding coupling. For definitiveness, we choose a lattice constant of  $a = 5.0 \text{ \AA}$ , distance between sites in each cell of  $1.7 \text{ \AA}$  in both materials, tight-binding coupling between the nearest-neighbor Wannier functions of  $t_{\text{odd}}^i = t_{\text{even}}^i = -3.0 \text{ eV}$ , and on-site energies of  $h_{\text{odd}}^A = 1.0 \text{ eV}$ ,  $h_{\text{even}}^A = 7.0$ ,  $h_{\text{odd}}^B = -3.0 \text{ eV}$ , and  $h_{\text{even}}^B = 3.0 \text{ eV}$ . The interfacial distance is  $a_{AB} = 7.7 \text{ \AA}$  and  $t_{AB} = 0.2 \text{ eV}$ . Those parameters are chosen to obtain semiconductors with identical electronic structure (6.0 eV gap and 3.7 eV bandwidth) but rigidly shifted in energy, resulting in a heterojunction where there is no spectral overlap among the bands. This ensures that the heterojunction is insulating to both an applied bias voltage and resonant photoexcitation, such that all charge transfer events are due to SCELl [28].

The laser pulse employed in the simulations is a few-cycle laser of central frequency  $\hbar\omega = 0.5 \text{ eV}$ , width  $\tau = 5.85 \text{ fs}$ , centered around  $t_c = 50 \text{ fs}$ , and carrier envelope phase (CEP)  $\phi = 0$ . A few-cycle laser is chosen to suppress the onset of dielectric breakdown [12,29,54] even for moderately strong fields. Such laser pulse is far detuned from electronic transitions in the system such that Stark effects dominate the

photoresponse. The vector potential associated with the laser pulse is of the form

$$\mathbf{A}_L(t) = \frac{E_0}{\omega} e^{-(t-t_c)^2/2\tau^2} \sin[\omega(t-t_c) + \phi] \hat{i}, \quad (3)$$

where  $E_0$  is the peak field amplitude. The associated electric field  $\mathbf{E}_L(t) = -\dot{\mathbf{A}}_L(t) = E_L(t)\hat{i}$  is given by

$$E_L(t) = \frac{E_0}{\omega} e^{-(t-t_c)^2/2\tau^2} \left\{ \frac{(t-t_c)}{\tau^2} \sin[\omega(t-t_c) + \phi] - \omega \cos[\omega(t-t_c) + \phi] \right\}. \quad (4)$$

This form guarantees that  $\mathbf{E}_L(t)$  remains an ac source even for few-cycle lasers as  $\int_{-\infty}^{\infty} \mathbf{E}_L(t) dt = \mathbf{A}_L(-\infty) - \mathbf{A}_L(\infty) = 0$ .

Since the Hamiltonian in Eq. (1) is a single-particle operator, the electronic properties of the system are characterized by the electronic reduced density matrix  $\rho_{n,m}(t) = \langle \Psi(t) | \hat{a}_n^\dagger \hat{a}_m | \Psi(t) \rangle$ , where  $|\Psi(t)\rangle$  is the many-body wave function. The dynamics of  $\rho_{n,m}(t)$  is determined by the Liouville-von Neumann equation

$$i\hbar \frac{d}{dt} \rho_{n,m}(t) = \langle [\hat{a}_n^\dagger \hat{a}_m, \hat{H}] \rangle, \quad (5)$$

with initial condition  $\rho_{nm}(0) = \sum_{\varepsilon} \langle \varepsilon | n \rangle \langle \varepsilon | m \rangle f(\varepsilon)$ , where  $|\varepsilon\rangle$  are the single-particle eigenstates of  $\hat{H}$  at time  $t = 0$ , and  $f(\varepsilon)$  is the initial Fermi distribution function. Equation (5) is numerically integrated from  $t = 0$  to 110 fs, using the predictor-corrector Adams-Moulton method with adaptive time step in the SUNDIALS package [74]. Snapshots of the key observables are recorded every  $\Delta t_{\text{obs}} = 0.01 \text{ fs}$ .

The electron transfer dynamics is monitored through changes in the total charge  $\Delta Q_i$  of each material. Specifically, we focus on

$$\Delta Q_A(t) = |e| \sum_{n \in A} [\rho_{nn}(t) - \rho_{nn}(0)], \quad (6a)$$

$$\Delta Q_B(t) = |e| \sum_{n \in B} [\rho_{nn}(t) - \rho_{nn}(0)]. \quad (6b)$$

Any  $A \rightarrow B$  electron transfer is monitored by

$$Q_{A \rightarrow B}(t) = \Delta Q_B(t). \quad (6c)$$

## III. RESULTS AND DISCUSSION

### A. SCELl basics

In the interest of clarity, we briefly summarize the main mechanism behind SCELl. The interaction of the  $AB$  heterojunction with the electric field of nonresonant light leads to a distortion of its electronic structure due to the Stark shifts. Specifically, the laser-matter interaction breaks the periodicity of the potential of the semiconductors that form the heterojunction [75–77], introducing equally spaced resonances in the energy spectrum [known as the Wannier-Stark ladder (WSL)], and localizes the electronic wave functions of the instantaneous Hamiltonian. To see this, it is convenient to focus on a tight-binding one-band model in the presence of a static electric field  $E$  [75–77]. For this model, the Wannier-Stark ladder eigenenergies are

$$\varepsilon_m = \varepsilon_0 + |e|maE, \quad (7)$$

where  $\varepsilon_0$  denotes the center of the energy band for the field-free model,  $m = \dots, -2, -1, 0, 1, 2, \dots$ ,  $a$  the lattice constant, and  $E$  the electric field. The interaction with the electric field fans out the energy levels in the band. In addition, this interaction localizes the electronic eigenfunctions by introducing a linear potential whose difference between consecutive sites is  $|e|aE$ . In fact, in the one-band model, the wave function of the Wannier-Stark state with energy  $\varepsilon_m$  is localized around site  $m$  and is given by  $|\Psi_m\rangle = \sum_n J_{n-m}(t_0/2|e|aE)|n\rangle$ , where  $J_n(x)$  is the Bessel function of the  $n$ th order and  $t_0$  is the tight-binding coupling between sites. The degree of localization increases as the electric field increases and thus the potential drop between consecutive sites increases.

In SCELl, the interaction of the  $AB$  heterojunction with the electric field of nonresonant light leads to a fanning out of the energy eigenstates of all bands. As a result of this distortion, transient resonances between energy levels belonging to the different bands of the semiconductors are formed. When the energy eigenstates involved in the transient resonances are VB levels of  $A$  and CB levels of  $B$ , quantum tunneling channels for  $A \rightarrow B$  electron transfer are opened. The quantum tunneling channels are particularly effective when the wave functions of the Wannier-Stark states involved overlap at the interface. The electric field amplitude at which the transient resonances that lead to  $A \rightarrow B$  electron transfer occur can be approximately obtained by assuming that all bands are independent of one another. Then, using Eq. (7), the transient resonances between the VB of  $A$  and the CB of  $B$  are formed when  $\varepsilon_m^A = \varepsilon_n^B$ , where  $\varepsilon_m^A$  is the energy of the Wannier-Stark state of material  $A$  localized at site  $m$ , and  $\varepsilon_n^B$  is the energy of the Wannier-Stark state of material  $B$  localized at site  $n$ . As a consequence, the electric field at which the transient resonances take place is

$$E = \frac{\varepsilon_0^A - \varepsilon_0^B}{x_m^A - x_n^B}, \quad (8)$$

where  $x_n^i = na$  is the position for site  $n$  of semiconductor  $i = A$  or  $B$ .

## B. Screening effects

To understand how SCELl is affected by screening effects generated by photogenerated charge displacements in the material, we introduced Maxwell's equations through the general boundary conditions of the field vectors at the interfaces. We assume that the laser incides perpendicular to the  $AB$  heterojunction, such that the linearly polarized electric field oscillates parallel to it. Thus, the laser polarizes the heterojunction and induces surface charges that create a screening field. To determine the effective electric field inside the heterojunction, we focus on the vacuum-heterojunction interface. From the condition of continuity of the normal component of the electric displacement field  $\mathbf{D}_\perp = \varepsilon_0 \mathbf{E}(t) + \mathbf{P}(t)$  between these two media,  $\mathbf{D}_{1,\perp} - \mathbf{D}_{2,\perp} = \sigma$ , it is possible to connect the electric field  $\mathbf{E}(t)$  inside the heterojunction with the incident laser field  $\mathbf{E}_L(t)$  in vacuum and the induced dielectric polarization density  $\mathbf{P}(t)$  in the heterojunction. For our system,  $\mathbf{D}_{k,\perp}$  represents the normal electric displacement for vacuum ( $k = 1$ ) and the  $AB$  heterojunction ( $k = 2$ ). Since the two media, i.e., vacuum and  $AB$  heterojunction, are dielectric materials, the free charge density  $\sigma = 0$ . Therefore,

the effective laser field inside the heterojunction is

$$\mathbf{E}(t) = \mathbf{E}_L(t) - \frac{\mathbf{P}(t)}{\varepsilon_0}. \quad (9)$$

Here, the induced polarization density is determined as  $\mathbf{P}(t) = \boldsymbol{\mu}(t)/V$ , where the dielectric's total volume is  $V = [(N_A + N_B)a + a_{AB}]a^2$  and  $\boldsymbol{\mu}(t) = \sum_{n=1}^{2N_j} [\rho_{n,n}(t) - 1]x_n \hat{i}$  is the dipole moment. Note that because the electronic structure of materials  $A$  and  $B$  is identical except for a rigid shift in energy, they have identical hyperpolarizabilities and their dielectric response coincides. As a consequence, from an electromagnetic perspective, there is no additional discontinuity in the electric field along the  $AB$  interface. This simplifying feature of the model allows us to employ the dipole approximation of laser-matter interactions in spite of the interface. Further note that considering the more general case, where the two materials have different dielectric response, requires an analysis of the underlying microscopic charge dynamics in the presence of spatially varying fields. This is beyond the state of the art of computational methods and we therefore conduct all simulations under electric dipole approximation. The results are expected to be informative of the screening expected for heterojunctions between two materials with similar permittivity in the range of frequencies employed in the photoexcitation.

Figure 1 compares the electron transfer dynamics with (red line) and without (blue line) screening for a laser pulse of  $\hbar\omega = 0.5$  eV,  $E_0 = 0.3$  V/Å, and  $\phi = 0$ . Screening reduces the amplitude of the electric field by 39% at its peak (upper panel). This reduction leads to a decrease in the number of induced transient resonances that open quantum tunneling channels for  $A \rightarrow B$  electron transfer. In this particular case, it causes a reduction of 57% of the charge that is transferred across the  $AB$  interface due to SCELl, as seen in the lower panel.

The upper panel of Fig. 2 compares the charge transfer  $Q_{A \rightarrow B}(t_f)$  as a function of field amplitude  $E_0$  of the incident laser pulse with (red line) and without (blue line) screening. Our results of  $Q_{A \rightarrow B}(t)$  are reported at time  $t_f = 68$  fs, which is a time in which the electric field of the light is already imperceptible and SCELl effects are complete. The lower panel quantifies the degree of screening of the laser pulse and its influence on SCELl as a function of  $E_0$ . The degree of screening is calculated as the reduction on the field amplitude at  $t = t_c$ . Notice that the screening increases with  $E_0$  for  $E_0 < 0.7$  V/Å, as seen in the lower panel of Fig. 2. Clearly, the screening reduces the net  $Q_{A \rightarrow B}(t_f)$  obtained for amplitudes  $E_0 < 0.7$  V/Å because it reduces the effective field experienced by the material and thus the number of effective quantum tunneling channels for  $A \rightarrow B$  electron transfer for a given  $E_0$ . Nevertheless, the mechanism behind SCELl remains intact. For this reason, the effect increases with  $E_0$  as the field opens additional quantum tunneling channels for  $A \rightarrow B$  electron transfer even in the presence of screening. Overall, we observe that the screening reduces the electron transfer  $Q_{A \rightarrow B}(t_f)$  on average 44% for  $E_0 \leq 0.7$  V/Å (see lower panel of Fig. 2).

The screening reduces the magnitude of the effective electric field and can also modify its shape. Figure 1 compares the electric field experienced by the heterojunction with and without screening for a laser pulse of  $E_0 = 0.3$  V/Å. Here,

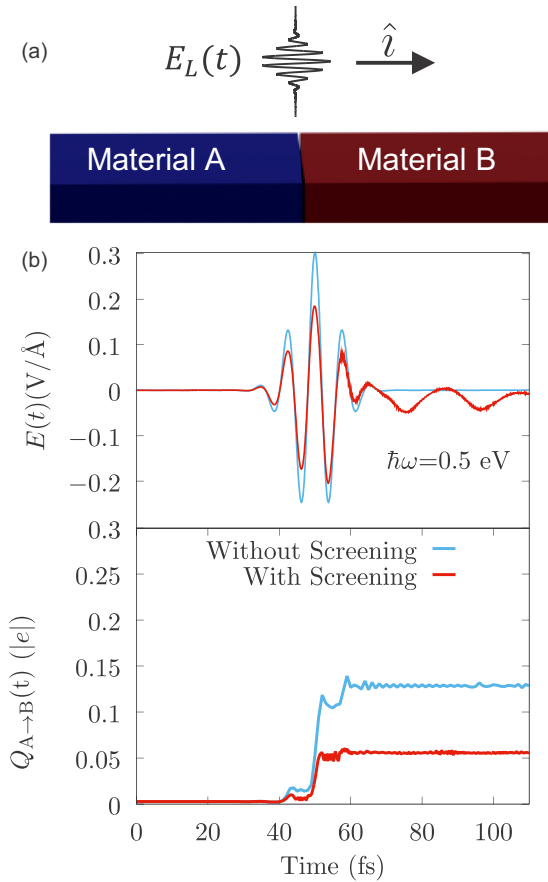


FIG. 1. Screening effects on the electron transfer dynamics across the  $AB$  heterojunction induced by non-resonant few-cycle laser pulses through Stark shifts. (a) Scheme of the heterojunction under the influence of a laser field polarized along direction  $\hat{i}$ . (b) The charge displacement induced by the laser pulse ( $\hbar\omega = 0.5$  eV,  $E_0 = 0.3$  V/ $\text{\AA}$  and  $\phi = 0$ ) generates a polarization in the material which diminishes the incident electric field of light (upper panel), leading to a reduction in the net charge transferred (lower panel).

one can notice that the screening just reduces the amplitude of the electric field, keeping the shape intact. However, for stronger fields  $E_0 > 0.55$  V/ $\text{\AA}$ , the harmonic mixing due to the nonlinear response of the material and the generation of real carriers leads to polarization contributions at frequencies larger than those of the incident pulse. The fast oscillation in  $\mathbf{P}(t)$  not only screens the electric field, but also modifies its shape; see Fig. 3.

We thus observe three regions of the response when screening is considered. In region I ( $E_0 \leq 0.093$  V/ $\text{\AA}$ ),  $Q_{A \rightarrow B}(t_f) = 0$  as the field is not intense enough to induce effective transient resonances that lead to  $A \rightarrow B$  electron transfer. In region II ( $0.093 < E_0 \leq 0.55$  V/ $\text{\AA}$ ), the screening reduces the amplitude of the electric field, on average, by 46%, while keeping its shape intact. In this region, the transient resonances that lead to charge transfer are mainly due to crossing between VB levels of A and CB levels of B. Last, in region III ( $E_0 > 0.55$  V/ $\text{\AA}$ ), screening reduces the electric field amplitude and modifies its shape, leading to a complicated dependence of  $Q_{A \rightarrow B}(t_f)$  on  $E_0$ .

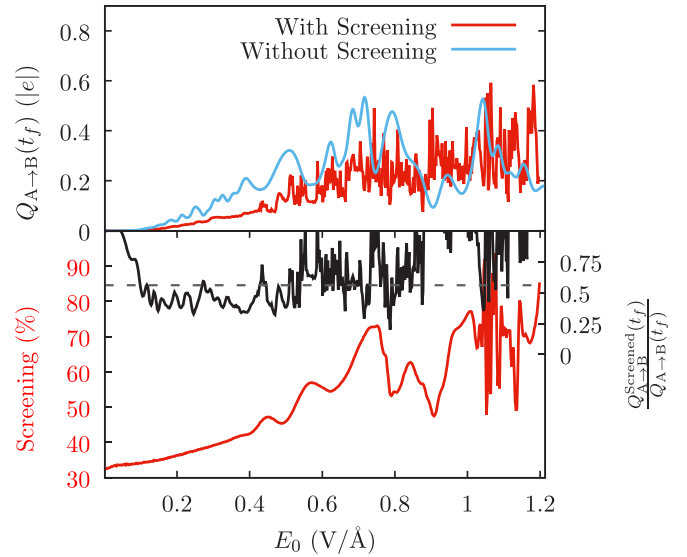


FIG. 2. Screening effects on the incident electric field of light and net charge transfer  $Q_{A \rightarrow B}(t_f)$ . The upper panel shows the charge transferred  $Q_{A \rightarrow B}(t_f)$  just after the pulse at time  $t_f = 68$  fs as a function of the incident laser pulse amplitude  $E_0$  with (red line) and without (blue line) screening effects. The lower panel shows the percentage of the electric field screening (red line) and the ratio between  $Q_{A \rightarrow B}(t_f)$  with and without screening (black line) as a function of  $E_0$ .

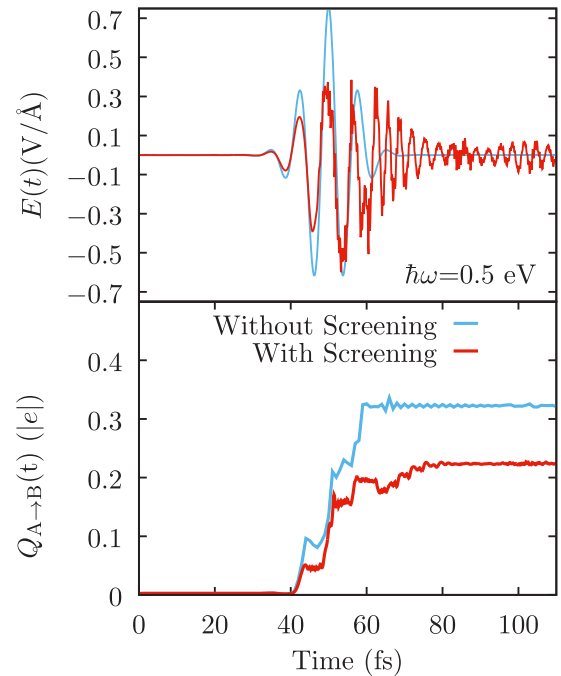


FIG. 3. Screening effects on the electric field and the electron transfer  $Q_{A \rightarrow B}(t)$  for a laser pulse of  $\hbar\omega = 0.5$  eV,  $E_0 = 0.75$  V/ $\text{\AA}$ , and  $\phi = 0$ . For  $E_0 > 0.55$  V/ $\text{\AA}$ , the induced dielectric polarization density not only diminishes the amplitude of the electric field, but also modifies its shape (upper panel). This effect reduces the charge transfer and introduces new features on the electron transfer dynamics (lower panel).

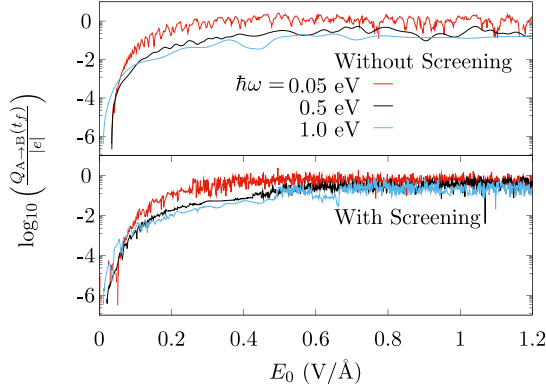


FIG. 4. Dependence of SCELI on laser parameters in the absence (upper panel) and in the presence (lower panel) of screening. Notice that in both cases, the charge transferred increases as the frequency of the laser pulse decreases, in agreement with a tunneling mechanism.

In the upper panels of Figs. 1 and 3, one can notice that there are oscillations that persist after pulse. These oscillations are the result of resonant processes in the photoexcitation that leave the heterojunction in a superposition of energy eigenstates.

To further understand the effects of screening on SCELI, we quantified the  $A \rightarrow B$  electron transfer induced by pulses with three different laser frequencies, but with the same number of cycles ( $\tau = \sqrt{2\pi}/\omega$ ). Figure 4 shows the behavior of the charge transfer  $Q_{A \rightarrow B}(t_f)$  as a function of the incident laser amplitude  $E_0$  for  $\hbar\omega = 0.05, 0.5$ , and  $1.0$  eV with and without screening. In all cases, in the regime in which there is an appreciable effect ( $E_0 > 0.076$  V/Å), decreasing the laser frequency increases the charge that is transferred. This is because, by decreasing  $\omega$ , one increases the time in which the relevant energy levels in the two materials are near resonance, thus enhancing the effectiveness of the tunneling events. Nevertheless, we also observe that for  $E_0 \leq 0.7$  V/Å, decreasing  $\omega$  increases the effects of screening. The average reduction of the charge transfer  $Q_{A \rightarrow B}(t_f)$  is 52% for  $\hbar\omega = 0.05$  eV, 44% for  $\hbar\omega = 0.5$  eV, and 35% for  $\hbar\omega = 1.0$  eV. This is because the response of the electrons of the heterojunction changes with  $\omega$ . For small  $\omega$ , the response of the electrons follows the instantaneous electric field, whereas for large  $\omega$ , the response follows the pulse envelope. Thus, the effects of  $\mathbf{P}(t)$  on the effective electric field increase as  $\omega$  decreases. From a SCELI perspective, it is advantageous to work with a lower frequency laser even when the screening effects increase. This is because the use of lower frequency pulses enhances the effectiveness of the quantum tunneling, which favors SCELI.

Figures 5(a) and 5(b) characterize the dependence of SCELI on the interfacial coupling strength  $t_{AB}$  with and without screening. As shown, in both cases, increasing  $t_{AB}$  monotonically increases the charge that is transferred for all  $E_0$  as it enhances the effectiveness of the quantum tunneling at the interface. However, we observe that as  $t_{AB}$  increases, the effects of screening increase. In fact, for  $t_{AB} = 0.05$  eV, the reduction in  $Q_{A \rightarrow B}(t_f)$  is, on average, 32% for  $E_0 \leq 0.7$  V/Å, whereas for  $t_{AB} = 0.9$  eV, the reduction is 47%. This is because as  $t_{AB}$  increases, the polarizability of the heterojunction and the amount of transferred charge also increases, leading

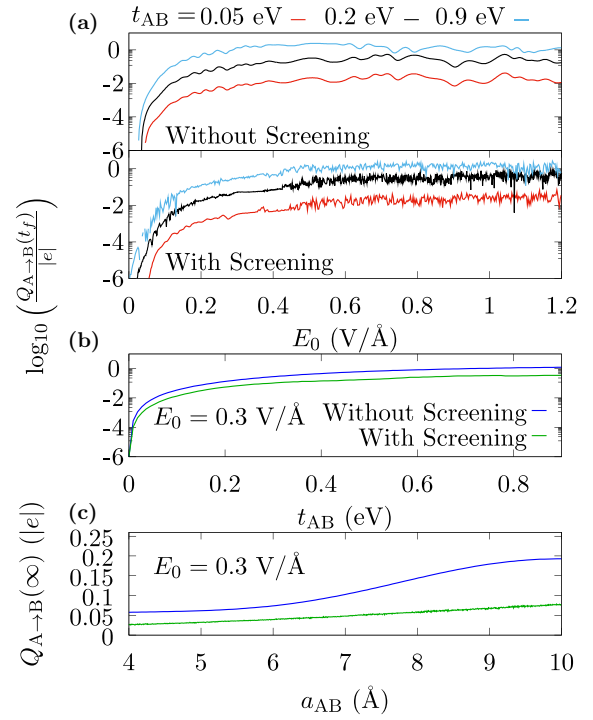


FIG. 5. Screening effects on the dependence of SCELI on the interfacial parameters. (a) Dependence on laser amplitude for three representative interfacial tight-binding couplings  $t_{AB}$ . (b) Dependence on  $t_{AB}$  for  $E_0 = 0.3$  V/Å. (c) Dependence on the interfacial distance for a fixed interfacial coupling  $t_{AB} = 0.2$  eV and  $E_0 = 0.3$  V/Å.

to an enhanced back reacting of the material on the effective electric field. Nonetheless, having larger value of  $t_{AB}$  is preferable, even when the screening effects increase, because SCELI is enhanced.

Additionally, Fig. 5(c) compares the dependence of SCELI on the interfacial distance  $a_{AB}$  with and without screening for a fixed  $t_{AB}$ . In both cases, increasing  $a_{AB}$  increases the charge transfer  $Q_{A \rightarrow B}(t_f)$  because this reduces the laser field amplitude required to create the transient resonances. To understand this, consider a minimal single-band model per material in the heterojunction. In the presence of a strong electric field, the electric field at which there is a transient resonance between a VB level of  $A$  localized at site  $m$  and CB level of  $B$  localized at a site  $n$  is given by Eq. (8). As  $a_{AB}$  increases,  $x_m^A - x_n^B$  increases, leading to a decrease in the  $E$  required to induce the transient resonance. Thus, increasing  $a_{AB}$  generally increases the charge transfer because the same pulse can induce more transient resonances that lead to  $A \rightarrow B$  electron transfer. In both cases,  $Q_{A \rightarrow B}(t_f)$  increases threefold when  $a_{AB}$  goes from 4 to 10 Å, which is consistent with the observation that the mechanism behind SCELI is not affected by screening.

In summary, we observe that screening in general reduces the amplitude of the effective electric field in the material for  $E_0 \leq 0.55$  V/Å, leading to a reduction in the charge transfer  $Q_{A \rightarrow B}(t_f)$  due to SCELI. However, the quantum tunneling mechanism described in Refs. [28,48] for the scheme of control and its dependence on the laser and material parameters is unaffected by the screening. For this reason, the effects

of screening can be partially overcome by increasing  $E_0$  up to a threshold  $E_0 = 0.55$  V/Å. Beyond this threshold, the effects of screening modify the shape of the effective electric field in the material, leading to a complicated dependence of  $Q_{A \rightarrow B}(t_f)$  on  $E_0$ .

### C. Band bending effects

To understand how band bending affects SCCLI, we employed a basic model for the electrostatic profile of the heterojunction upon thermal equilibration given by the so-called depletion approximation [72,73]. This approximation assumes that there exist depletion regions on both sides of the junction in which the electron and hole densities change exponentially with position. Outside these depletion regions, the appropriate electrostatic potential and electron and hole concentrations are those that would exist in the absence of the heterojunction. Here, we use the form of the electrostatic potential,  $V(x) = k_B T \sinh^{-1}(\frac{x}{2L_a})$ , for a neutral  $p$ - $n$  junction detailed in Ref. [72], where  $L_a$  is the length of the depletion region,  $k_B$  the Boltzmann constant, and  $T$  the temperature (we choose  $T = 300$  K). For the  $AB$  heterojunction, the electrostatic potential at the Wannier function  $n$  is thus

$$V_{nm} = k_B T \sinh^{-1} \left( \frac{na + a_{AB}/2}{sa + a_{AB}} \right), \quad (10)$$

where  $s$  is the number of unit cells in the depletion region. In the presence of this additional contribution, the Hamiltonian of each semiconductor of the heterojunction becomes

$$\hat{H}'_i = \sum_{n=1}^{2N_i} [h_{nm}^i + |e|E(t)x_n + V_{nm}] \hat{a}_n^\dagger \hat{a}_n + \sum_{(n,m)} h_{nm}^i \langle \hat{a}_n^\dagger \hat{a}_m + \text{H.c.} \rangle. \quad (11)$$

As shown in Figs. 6(a) and 6(b), this additional term in the Hamiltonian shifts the electric field amplitude needed to create the transient resonances behind SCCLI and also modulates their effectiveness. This causes a change in the charge that is transferred,  $Q_{A \rightarrow B}(t_f)$ , by the same laser pulse. To understand this shift in the required field amplitude, consider a minimal single-band model per material in the heterojunction. In this case, since we are interested in the  $A \rightarrow B$  electron transfer, we only consider VB of  $A$  and CB of  $B$ . The value of the electric field at which there is a crossing between a level localized at site  $n$  of  $A$  and site  $m$  of  $B$  is given by Eq. (8). When the band bending is taken into account, this value is modified to  $E = \frac{(h_{nm}^A + V_{nm}) - (h_{nm}^B + V_{nm})}{x_n^A - x_m^B}$ . With band bending, the energy difference in the numerator decreases because the energy eigenstates of the VB of  $A$  localized at the depletion region increase their energy due to the electrostatic potential of Eq. (10), while the energy eigenstates of the CB of  $B$  decrease their energy. Since  $x_n^A - x_m^B$  remains constant, the required field amplitude to induce the transient resonances decreases. In Fig. 6(b), the crossing shown is shifted from 0.65 to 0.61 V/Å, and the gap for this specific crossing increases from 0.28 to 0.31 eV (for other crossings, the energy gap can decrease too).

Figure 7 shows the effects of band bending on SCCLI. We observe that band bending mildly increases the effect of SCCLI for some values of  $E_0$  and mildly decreases the effect for others. Specifically, band bending has a bigger impact on

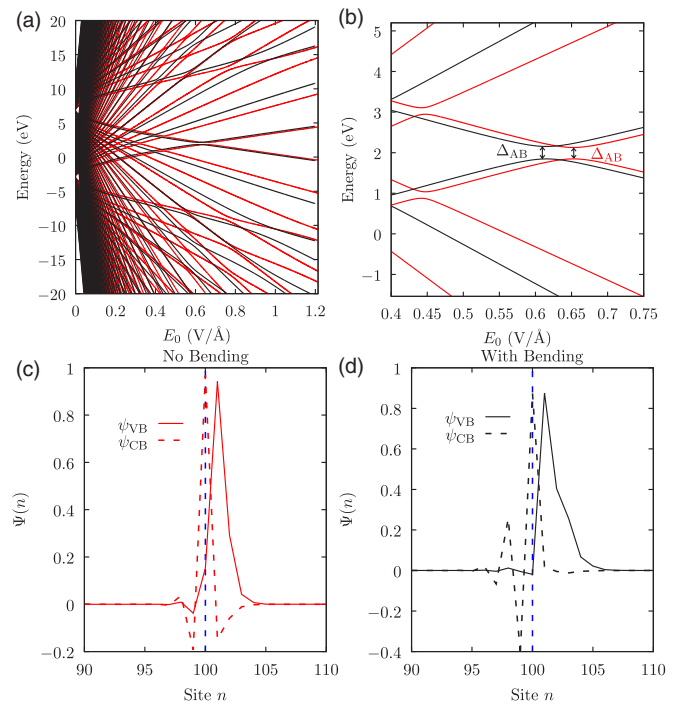


FIG. 6. Band bending effects on SCCLI. (a) Laser-dressed eigenenergies obtained by diagonalizing the Hamiltonian in Eq. (1) for fixed electric field amplitude  $E_0$  with (black lines) and without (red lines) band bending for  $s = 40$ . (b) Detail of an avoided crossing that leads to  $A \rightarrow B$  electron transfer. (c),(d) Overlap of the diabatic wave functions of the energy levels in (b).

SCCLI for  $E_0 \leq 0.2$  V/Å, where  $Q_{A \rightarrow B}(t_f)$  increases due to the decrease in the required field amplitude to induce transient resonances between VB of  $A$  and CB of  $B$  that lead to  $A \rightarrow B$  electron transfer. This leads to more quantum tunneling channels for interfacial electron transfer being opened for the same laser pulse. In turn, for the case with band bending plus screening,  $Q_{A \rightarrow B}(t_f)$  decreases, on average, 41% for  $E_0 \leq 0.46$  V/Å. This reduction is due to the effect of screening on the effective electric field experienced by the material. Thus, the screening dominates over band bending and play a determining role in SCCLI. For  $E_0 > 0.46$  V/Å, the  $B \rightarrow A$  electron transfer process plays a major role because band bending also modifies the required field amplitude to induce transient resonances between VB of  $B$  and CB of  $A$ . This process along with interband Zener tunneling lead to the observed complex dynamics for  $E_0 > 0.46$  V/Å.

Figure 7(b) shows the dependence of SCCLI on the depletion length  $s$  for the case with (red line) and without (blue lines) screening. In both cases, we observe that the band bending effects are approximately independent for  $s > 20$  and have a mild effect on the SCCLI dynamics. This shows that the behavior for  $s = 40$  in Figs. 7(a) and 7(b) is representative of interfaces of varying sharpness.

## IV. CONCLUSIONS

In this work, we investigated the effects of screening and band bending on SCCLI. The screening was introduced by Maxwell's equations through the general boundary conditions

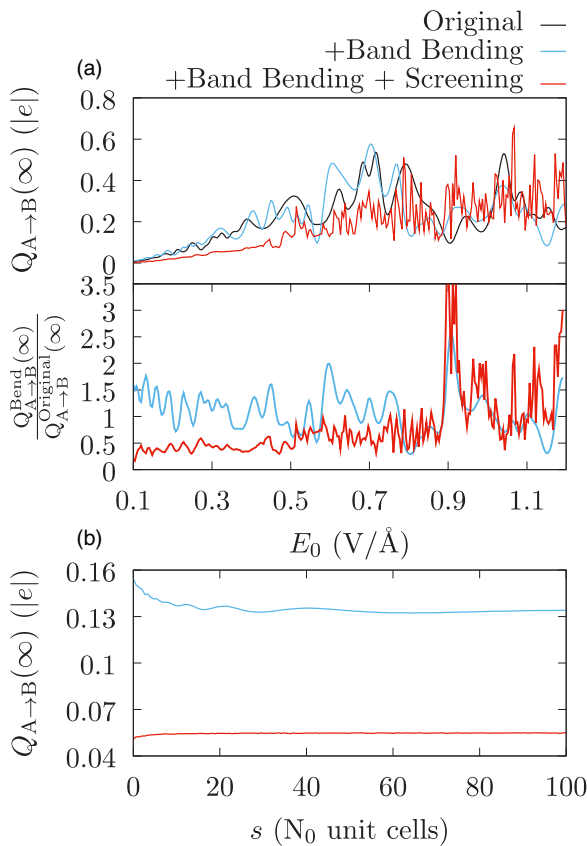


FIG. 7. Effect of interfacial band bending on SCEL. (a) Charge transferred as a function of the laser amplitude for an atomically sharp interface (black), and a 40-unit-cell interface with (red) and without (blue) screening effects. The bottom panel details the ratio of the charge transfer  $Q_{AB}(t_f)$  with respect to the atomically sharp interface in both cases. (b) Transferred charge as a function of the number of unit cells  $s$  involved in the interface for a laser pulse with  $\hbar\omega = 0.5$  eV,  $E_0 = 0.25$  V/ $\text{\AA}$ .

on the field vectors at the interfaces. In turn, band bending was included through an electrostatic interfacial given by the depletion approximation for neutral  $p$ - $n$  junctions.

We observe that the quantum tunneling mechanism behind SCEL is unaffected by band bending and screening. However, the net charge transfer  $Q_{AB}(t_f)$  is affected by these effects. In fact, when only screening is considered,  $Q_{AB}(t_f)$  is reduced, on average, 44% for  $E_0 \leq 0.7$  V/ $\text{\AA}$ . In turn,  $Q_{AB}(t_f)$  is mildly affected when only band bending is considered. When both effects are taken into account, the net charge transfer is reduced, on average, 41% for  $E_0 \leq 0.46$  V/ $\text{\AA}$ . The results show that screening dominates over band bending and plays a determining role in SCEL. Nevertheless, its effects on SCEL can be partially overcome by increasing the field amplitude  $E_0$  of the laser pulse up to a threshold  $E_0 = 0.55$  V/ $\text{\AA}$ .

Here, we have demonstrated that the shape of the electric field of light is modified by the screening effect for large field amplitudes. This implies that schemes of control that rely on the shape of the laser pulse, such as laser-induced symmetry breaking [7–12,17,18,20,21,26,30,48], can be limited by screening effects as the schemes can become uncontrollable for large field amplitudes for which the screening modifies the intended shape of the incident light pulse.

We point out that in the employed model, the electric field is isotropic along the  $AB$  heterojunction since materials  $A$  and  $B$  have the same dielectric response. The more general case where the two materials have different permittivity requires an analysis of the underlying microscopic charge dynamics in the presence of spatially varying fields, which go beyond the electric dipole approximation of laser-matter interactions.

Throughout, we demonstrate that SCEL survives under realistic conditions and can be used to control the electron across interfaces. As such, SCEL can be employed for the development of ultrafast electronics and optical actuators and exemplifies the robustness of the Stark-based strategies for the laser control of electrons.

## ACKNOWLEDGMENTS

This study is based on the work supported by the National Science Foundation under Grant No. CHE-1553939.

- [1] M. Shapiro and P. Brumer, *Quantum Control of Molecular Processes*, 2nd ed. (Wiley-VCH, Weinheim, 2012).
- [2] S. A. Rice and M. Zhao, *Optical Control of Molecular Dynamics* (Wiley, New York, 2000).
- [3] F. Krausz and M. Ivanov, *Rev. Mod. Phys.* **81**, 163 (2009).
- [4] G. Fleming and M. Ratner, *Phys. Today* **61**(7), 28 (2008).
- [5] A. D. Bandrauk, Molecules in laser fields, in *Frontiers of Chemical Dynamics*, edited by E. Yurtsever (Springer Netherlands, Dordrecht, 1995), pp. 131–150.
- [6] K. Ohmori, *Annu. Rev. Phys. Chem.* **60**, 487 (2009).
- [7] T. L. Cocker, D. Peller, P. Yu, J. Repp, and R. Huber, *Nature (London)* **539**, 263 (2016).
- [8] V. Jelic, K. Iwaszczuk, P. H. Nguyen, C. Rathje, G. J. Hornig, H. M. Sharum, J. R. Hoffman, M. R. Freeman, and F. A. Hegmann, *Nat. Phys.* **13**, 591 (2017).
- [9] T. Rybka, M. Ludwig, M. F. Schmalz, V. Knittel, D. Brida, and A. Leitenstorfer, *Nat. Photon.* **10**, 667 (2016).
- [10] T. Higuchi, C. Heide, K. Ullmann, H. B. Weber, and P. Hommelhoff, *Nature (London)* **550**, 224 (2017).
- [11] A. Schiffrin, T. Paasch-Colberg, N. Karpowicz, V. Apalkov, D. Gerster, S. Mühlbrandt, M. Korbman, J. Reichert, M. Schultze, S. Holzner, J. V. Barth, R. Kienberger, R. Ernstorfer, V. S. Yakovlev, M. I. Stockman, and F. Krausz, *Nature (London)* **493**, 70 (2013).
- [12] M. Schultze, E. M. Bothschafter, A. Sommer, S. Holzner, W. Schweinberger, M. Fiess, M. Hofstetter, R. Kienberger, V. Apalkov, V. S. Yakovlev, M. I. Stockman, and F. Krausz, *Nature (London)* **493**, 75 (2013).
- [13] I. Franco, M. Shapiro, and P. Brumer, *Phys. Rev. Lett.* **99**, 126802 (2007).
- [14] P. B. Corkum and F. Krausz, *Nat. Phys.* **3**, 381 (2007).

- [15] C. Heide, T. Boolakee, T. Higuchi, H. B. Weber, and P. Hommelhoff, *New J. Phys.* **21**, 045003 (2019).
- [16] S. Ghimire, A. D. DiChiara, E. Sistrunk, P. Agostini, L. F. DiMauro, and D. A. Reis, *Nat. Phys.* **7**, 138 (2011).
- [17] M. Krüger, M. Schenk, M. Förster, and P. Hommelhoff, *J. Phys. B* **45**, 074006 (2012).
- [18] L. Chen, Y. Zhang, G. H. Chen, and I. Franco, *Nat. Commun.* **9**, 2070 (2018).
- [19] M. Hohenleutner, F. Langer, O. Schubert, M. Knorr, U. Huttner, S. W. Koch, M. Kira, and R. Huber, *Nature (London)* **523**, 572 (2015).
- [20] G. Vampa, T. J. Hammond, N. Thiré, B. E. Schmidt, F. Légaré, C. R. McDonald, T. Brabec, D. D. Klug, and P. B. Corkum, *Phys. Rev. Lett.* **115**, 193603 (2015).
- [21] G. Vampa, T. J. Hammond, N. Thiré, B. E. Schmidt, F. Légaré, C. R. McDonald, T. Brabec, and P. B. Corkum, *Nature (London)* **522**, 462 (2015).
- [22] T. T. Luu, M. Garg, S. Y. Kruchinin, A. Moulet, M. T. Hassan, and E. Goulielmakis, *Nature (London)* **521**, 498 (2015).
- [23] M. Garg, M. Zhan, T. T. Luu, H. Lakhotia, T. Klostermann, A. Guggenmos, and E. Goulielmakis, *Nature (London)* **538**, 359 (2016).
- [24] N. Yoshikawa, T. Tamaya, and K. Tanaka, *Science* **356**, 736 (2017).
- [25] H. Liu, Y. Li, Y. S. You, S. Ghimire, T. F. Heinz, and D. A. Reis, *Nat. Phys.* **13**, 262 (2017).
- [26] J. Reimann, S. Schlauderer, C. P. Schmid, F. Langer, S. Baierl, K. A. Kokh, O. E. Tereshchenko, A. Kimura, C. Lange, J. Güdde, U. Höfer, and R. Huber, *Nature (London)* **562**, 396 (2018).
- [27] F. Langer, C. P. Schmid, S. Schlauderer, M. Gmitra, J. Fabian, P. Nagler, C. Schüller, T. Korn, P. G. Hawkins, J. T. Steiner, U. Huttner, S. W. Koch, M. Kira, and R. Huber, *Nature (London)* **557**, 76 (2018).
- [28] A. J. Garzón-Ramírez and I. Franco, *Phys. Rev. B* **98**, 121305(R) (2018).
- [29] O. Schubert, M. Hohenleutner, F. Langer, B. Urbanek, C. Lange, U. Huttner, D. Golde, T. Meier, M. Kira, S. W. Koch, and R. Huber, *Nat. Photon.* **8**, 119 (2014).
- [30] C. Heide, T. Higuchi, H. B. Weber, and P. Hommelhoff, *Phys. Rev. Lett.* **121**, 207401 (2018).
- [31] S. Y. Kruchinin, M. Korbman, and V. S. Yakovlev, *Phys. Rev. B* **87**, 115201 (2013).
- [32] Y.-C. Han, K.-J. Yuan, W.-H. Hu, and S.-L. Cong, *J. Chem. Phys.* **130**, 044308 (2009).
- [33] H. Nagai, H. Ohmura, F. Ito, T. Nakanaga, and M. Tachiya, *J. Chem. Phys.* **124**, 034304 (2006).
- [34] M. Shapiro and P. Brumer, *Rep. Prog. Phys.* **66**, 859 (2003).
- [35] P. Brumer and M. Shapiro, *Annu. Rev. Phys. Chem.* **43**, 257 (1992).
- [36] R. J. Gordon and S. A. Rice, *Annu. Rev. Phys. Chem.* **48**, 601 (1997).
- [37] J. G. Underwood, M. Spanner, M. Y. Ivanov, J. Mottershead, B. J. Sussman, and A. Stolow, *Phys. Rev. Lett.* **90**, 223001 (2003).
- [38] B. J. Sussman, D. Townsend, M. Y. Ivanov, and A. Stolow, *Science* **314**, 278 (2006).
- [39] M. E. Corrales, R. de Nalda, and L. Bañares, *Nat. Commun.* **8**, 1345 (2017).
- [40] A. Haché, Y. Kostoulas, R. Atanasov, J. L. P. Hughes, J. E. Sipe, and H. M. van Driel, *Phys. Rev. Lett.* **78**, 306 (1997).
- [41] H. Tahara and Y. Kanemitsu, *Phys. Rev. B* **90**, 245203 (2014).
- [42] S. Priyadarshi, K. Pierz, and M. Bieler, *Phys. Rev. Lett.* **109**, 216601 (2012).
- [43] S. Priyadarshi, K. Pierz, and M. Bieler, *Appl. Phys. Lett.* **102**, 112102 (2013).
- [44] E. Dupont, P. B. Corkum, H. C. Liu, M. Buchanan, and Z. R. Wasilewski, *Phys. Rev. Lett.* **74**, 3596 (1995).
- [45] C. Zhuang, C. R. Paul, X. Liu, S. Maneshi, L. S. Cruz, and A. M. Steinberg, *Phys. Rev. Lett.* **111**, 233002 (2013).
- [46] A. J. White, U. Peskin, and M. Galperin, *Phys. Rev. B* **88**, 205424 (2013).
- [47] N. T. Phuc and A. Ishizaki, *Phys. Rev. B* **99**, 064301 (2019).
- [48] A. J. Garzón-Ramírez and I. Franco, *J. Chem. Phys.* **153**, 044704 (2020).
- [49] B. Gu and I. Franco, *Phys. Rev. A* **98**, 063412 (2018).
- [50] T. Szidarovszky, A. G. Császár, G. J. Halász, and A. Vibók, *Phys. Rev. A* **100**, 033414 (2019).
- [51] M. Reutzell, A. Li, and H. Petek, *Phys. Rev. X* **9**, 011044 (2019).
- [52] M. Reutzell, A. Li, B. Gumhalter, and H. Petek, *Phys. Rev. Lett.* **123**, 017404 (2019).
- [53] A. Srivastava, R. Srivastava, J. Wang, and J. Kono, *Phys. Rev. Lett.* **93**, 157401 (2004).
- [54] M. Lenzen, J. Krüger, S. Sartania, Z. Cheng, C. Spielmann, G. Mourou, W. Kautek, and F. Krausz, *Phys. Rev. Lett.* **80**, 4076 (1998).
- [55] I. R. Solá, B. Y. Chang, J. Santamaría, V. S. Malinovsky, and J. L. Krause, *Phys. Rev. Lett.* **85**, 4241 (2000).
- [56] H. Niikura, P. B. Corkum, and D. M. Villeneuve, *Phys. Rev. Lett.* **90**, 203601 (2003).
- [57] E. J. Sie, J. W. McIver, Y.-H. Lee, L. Fu, J. Kong, and N. Gedik, *Nat. Mater.* **14**, 290 (2014).
- [58] A. Kar and I. Franco, *J. Chem. Phys.* **146**, 214107 (2017).
- [59] B. Gu and I. Franco, *J. Phys. Chem. Lett.* **8**, 4289 (2017).
- [60] B. Gu and I. Franco, *J. Phys. Chem. Lett.* **9**, 773 (2018).
- [61] W. Hu, B. Gu, and I. Franco, *J. Chem. Phys.* **148**, 134304 (2018).
- [62] S. Sze, *Physics of Semiconductor Devices*, 2nd ed. (Wiley, New York, 1981).
- [63] E. F. Schubert, *Physical Foundations of Solid-State Devices* (Department of Electrical, Computer, and Systems Engineering, Rensselaer Polytechnic Institute, Troy, New York, 2006).
- [64] T. Nakayama, Y. Kangawa, and K. Shiraishi, Atomic structures and electronic properties of semiconductor interfaces, in *Comprehensive Semiconductor Science and Technology*, Vol. 1, edited by P. Bhattacharya, R. Fornari, and H. Kamimura (Elsevier, New York, 2011), pp. 113–174.
- [65] J. Tersoff, *Phys. Rev. B* **30**, 4874 (1984).
- [66] Z. Zhang and J. T. Yates, *Chem. Rev.* **112**, 5520 (2012).
- [67] W. Mönch, Electronic properties of semiconductor interfaces, in *Springer Handbook of Electronic and Photonic Materials*, edited by S. Kasap and P. Capper (Springer International, Cham, 2017), pp. 1.
- [68] F. Della Sala, A. Di Carlo, P. Lugli, F. Bernardini, V. Fiorentini, R. Scholz, and J.-M. Jancu, *Appl. Phys. Lett.* **74**, 2002 (1999).
- [69] M. Korbman, S. Y. Kruchinin, and V. S. Yakovlev, *New J. Phys.* **15**, 013006 (2013).

- [70] G. Wachter, C. Lemell, J. Burgdörfer, S. A. Sato, X.-M. Tong, and K. Yabana, *Phys. Rev. Lett.* **113**, 087401 (2014).
- [71] T. Paasch-Colberg, S. Y. Kruchinin, Özge Sağlam, S. Kapsler, S. Cabrini, S. Muehlbrandt, J. Reichert, J. V. Barth, R. Ernstorfer, R. Kienberger, V. S. Yakovlev, N. Karpowicz, and A. Schiffrin, *Optica* **3**, 1358 (2016).
- [72] W. Shockley, *Bell Labs Tech. J* **28**, 435 (1949).
- [73] J. M. Pimbley, *IEEE Trans. Electron Devices* **35**, 1957 (1988).
- [74] A. C. Hindmarsh, P. N. Brown, K. E. Grant, S. L. Lee, R. Serban, D. E. Shumaker, and C. S. Woodward, *ACM Trans. Math. Software (TOMS)* **31**, 363 (2005).
- [75] G. C. Stey and G. Gusman, *J. Phys. C* **6**, 650 (1973).
- [76] M. Glück, A. R. Kolovsky, and H. J. Korsch, *Phys. Rep* **366**, 103 (2002).
- [77] T. Hartmann, F. Keck, H. J. Korsch, and S. Mossmann, *New J. Phys.* **6**, 2 (2004).